Youlong Chen
International Center for Applied Mechanics,
SV Laboratory,
School of Aerospace,
Xi'an Jiaotong University,
No. 28, Xianning West Road,
Xi'an, Shaanxi 710049, China
e-mail: cyl.900125@stu.xjtu.edu.cn

Yong Zhu
Department of Mechanical and
Aerospace Engineering,
North Carolina State University,
Engineering Building 3,
Rm 3238 (Centennial Campus),
911 Oval Drive,
Raleigh, NC 27695
e-mail: yong_zhu@ncsu.edu

Xi Chen[1]
Fellow ASME
Columbia Nanomechanics Research Center,
Department of Earth and
Environmental Engineering,
Columbia University,
500 West 120th Street,
New York, NY 10027
e-mail: xichen@columbia.edu

Yilun Liu[1]
State Key Laboratory for Strength and
Vibration of Mechanical Structures,
School of Aerospace,
Xi'an Jiaotong University,
No. 28, Xianning West Road,
Xi'an, Shaanxi 710049, China
e-mail: yilunliu@mail.xjtu.edu.cn

Mechanism of the Transition From In-Plane Buckling to Helical Buckling for a Stiff Nanowire on an Elastomeric Substrate

In this work, the compressive buckling of a nanowire partially bonded to an elastomeric substrate is studied via finite-element method (FEM) simulations and experiments. The buckling profile of the nanowire can be divided into three regimes, i.e., the in-plane buckling, the disordered buckling in the out-of-plane direction, and the helical buckling, depending on the constraint density between the nanowire and the substrate. The selection of the buckling mode depends on the ratio d/h, where d is the distance between adjacent constraint points and h is the helical buckling spacing of a perfectly bonded nanowire. For $d/h > 0.5$, buckling is in-plane with wavelength $\lambda = 2d$. For $0.27 < d/h < 0.5$, buckling is disordered with irregular out-of-plane displacement. While, for $d/h < 0.27$, buckling is helical and the buckling spacing gradually approaches to the theoretical value of a perfectly bonded nanowire. Generally, the in-plane buckling induces smaller strain in the nanowire, but consumes the largest space. Whereas the helical mode induces moderate strain in the nanowire, but takes the smallest space. The study may shed useful insights on the design and optimization of high-performance stretchable electronics and three-dimensional complex nanostructures. [DOI: 10.1115/1.4032573]

1 Introduction

Recently, the buckling mechanism has been widely used in the fabrication of stretchable electronics and three-dimensional complex microstructures [1–7]. In stretchable electronics, the fragile and stiff elements (e.g., silicon, metal films, or wires) are usually placed on an elastomeric substrate and precompressed to some fundamental buckling modes. By taking advantage of the buckling deformation, the compressive strain of the stiff/brittle element is significantly released and replaced by a relative small bending strain. Therefore, very large deformability of the stretchable electronics can be achieved by stretching the buckled elements to their original configurations, examples include the noncoplanar mesh design composed of semiconductor islands and buckled thin interconnects on elastomeric substrates which can achieve large and reversible tensile deformation (exceeding 100%) [8]. Buckling of thin film or nanofiber on a curved substrate can generate very complex patterns, e.g., helical, springlike or gearlike structures, which can be used to fabricate complex structures at micro or even nanoscales [9]. The compressive buckling of the initially curved slender wire or thin film with partial bonding to the elastomeric substrate can generate complex three-dimensional micro/nanostructures, which hold great potential applications in advanced micro/nanosystems technologies [1,2].

Nanowires, especially the silicon nanowires (SiNWs), are one of the key building blocks for nanoscale electronic, photonic and electromechanical devices due to their excellent properties in mechanics, electronics, and optics [10–14]. A number of flexible (mostly bendable) electronics have been developed by using the SiNWs [4,15–17]. In order to attain large bending or stretching deformation, the SiNWs are usually retained in the buckled profile on top of a prestretched Poly-dimethylsiloxane (PDMS) substrate. After releasing the prestrain in the PDMS substrate, the SiNWs buckle into either an in-plane mode or a three-dimensional helical coil form, depending on the adhesion strength between the SiNWs and the PDMS substrate [4]. In experiments, the PDMS substrate with SiNWs are radiated by ultraviolet/ozone (UVO) to generate chemical bonds between them, where the adhesion strength increases with the UVO treatment time [18,19]. However, the underling mechanism of the buckling mode transition from the in-plane mode to the helical mode has not yet been well explained.

The compressive buckling of a stiff nanowire on an elastomeric substrate has been studied in previous literature, examples such as the in-plane buckling, out-of-plane buckling, and helical buckling of the nanowire [16,20,21]. In these works, the nanowires were assumed perfectly bonded to the elastomeric substrates throughout deformation, and the effect of the interface debonding on the buckling behaviors was ignored. However, for the buckling of the SiNWs on the PDMS substrate, the UVO treatment time plays an

[1]Corresponding authors.

Contributed by the Applied Mechanics Division of ASME for publication in the Journal of Applied Mechanics. Manuscript received December 2, 2015; final manuscript received January 22, 2016; published online February 10, 2016. Editor: Yonggang Huang.

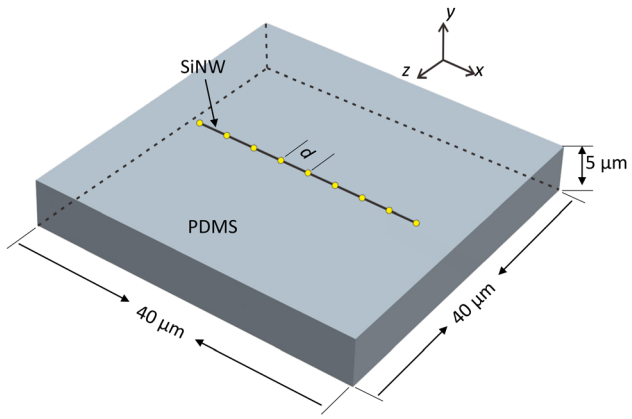

Fig. 1 Model of a SiNW partially bonded to the PDMS substrate. The dots represent the constraint between the SiNW and the PDMS substrate and the distance between the adjacent constraint points. A uniaxial compression is applied to the PDMS substrate in *x* direction.

important role in the buckling mode of the SiNWs. The SiNWs may partially debond from the PDMS substrate during compressive buckling, especially with less UVO treatment time. Although the competition between the in-plane buckling mode and out-of-plane buckling mode of SiNW has been studied in recent literature, the selection of the buckling mode is determined by minimum moment of inertia due to the noncircular cross section of the SiNW [22]. In this work, the buckling behaviors of the SiNWs partially bonded to the PDMS substrate are studied to explore the mechanism of the transition from in-plane buckling to helical buckling.

2 Model and Method

As shown in Fig. 1, a SiNW is placed on the PDMS substrate and a uniaxial compression is applied on the PDMS substrate in x direction (the axial direction of SiNW); this is equivalent to releasing the prestrain in the PDMS substrate. Only some definite dots in the SiNW are constrained to the PDMS substrate, so as to represent the partial bonding between the SiNW and the PDMS substrates. The constraint between the SiNW and the PDMS is the node-type-constraint, which means the corresponding nodes in the SiNW and the PDMS have the same displacement. Indeed, we have checked different types of constraints, e.g., node-type constraint, element-type-constraint, and the influence to the critical buckling strain of SiNW is negligible.

The distance between adjacent constraint points is d, as shown in Fig. 1. As shown in our previous study, the compression buckling mode of a perfectly bonded SiNW ($d/h = 0$) is helical and the buckling spacing is $h = 7.89R(E_{NW}/\bar{E}_S)^{1/4}$ determined by the

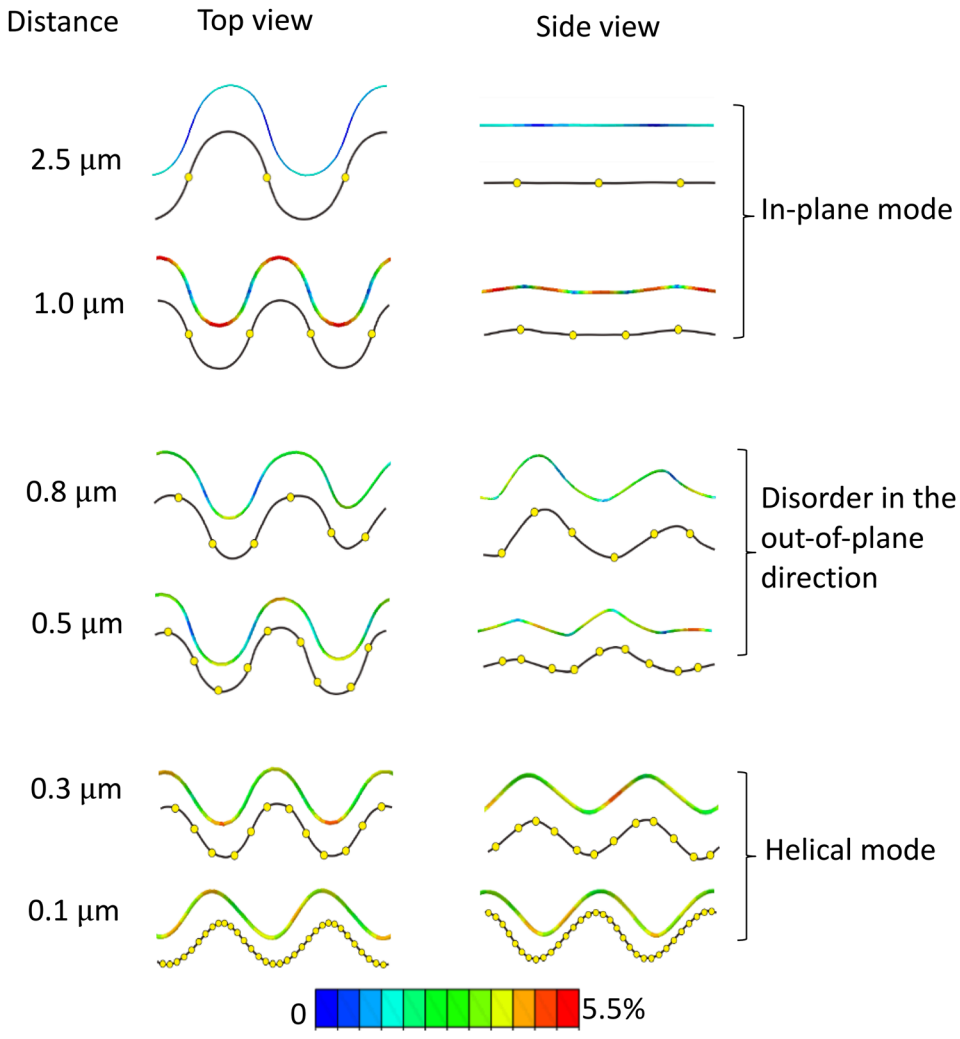

Fig. 2 The buckling modes of the SiNW partially bonded to a PDMS substrate. The dots represent the constraints (bonded sites) between the SiNW and the PDMS substrate. Color contour of the maximum principal strain in the buckled configuration is given.

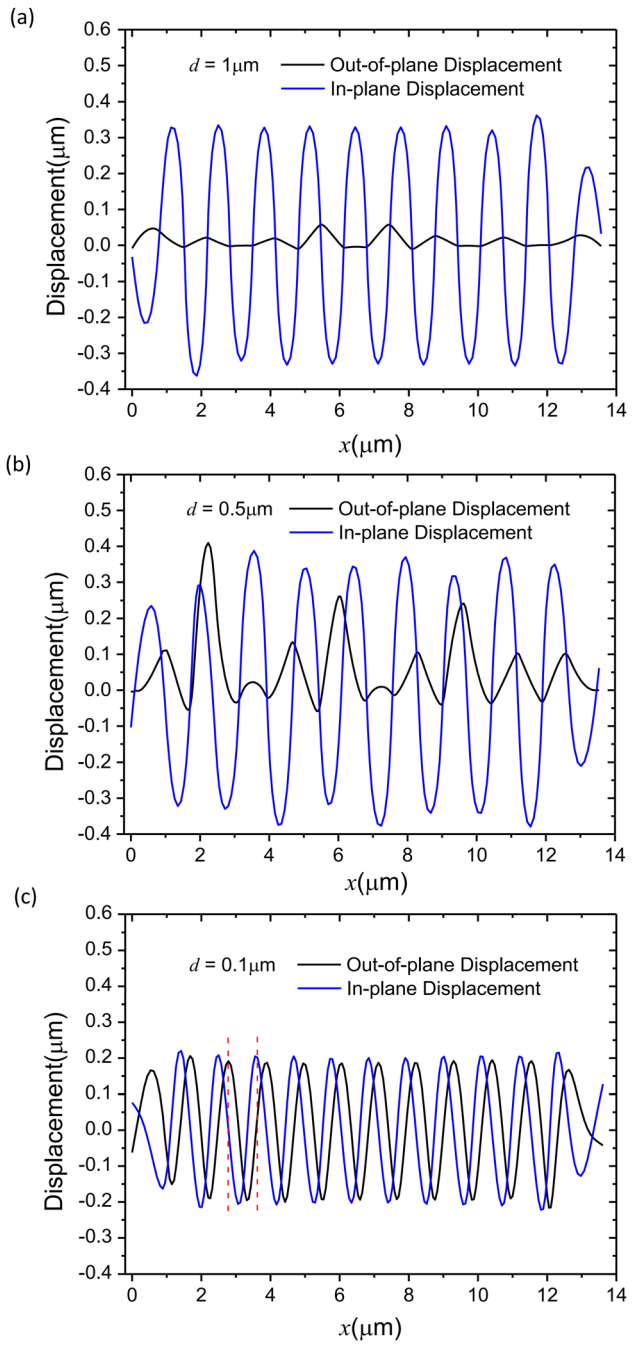

Fig. 3 The in-plane (u_z) and out-of-plane (u_y) displacements of SiNW corresponding to different modes in Fig. 2 ($d = 1\,\mu$m, $d = 0.5\,\mu$m, and $d = 0.1\,\mu$m), respectively

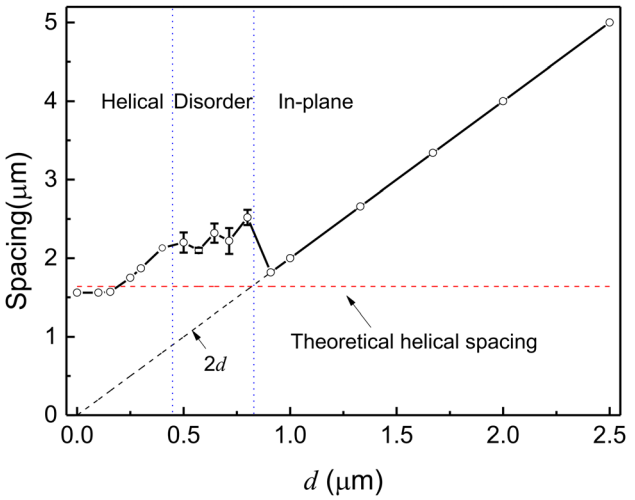

Fig. 4 The buckling wavelength of SiNW for different constraint densities. The horizontal dashed line indicates the theoretical buckling spacing *h* of the perfectly bonded SiNW and the oblique dashed line is 2*d*. Error bars are given for the out-of-plane disordered buckling mode.

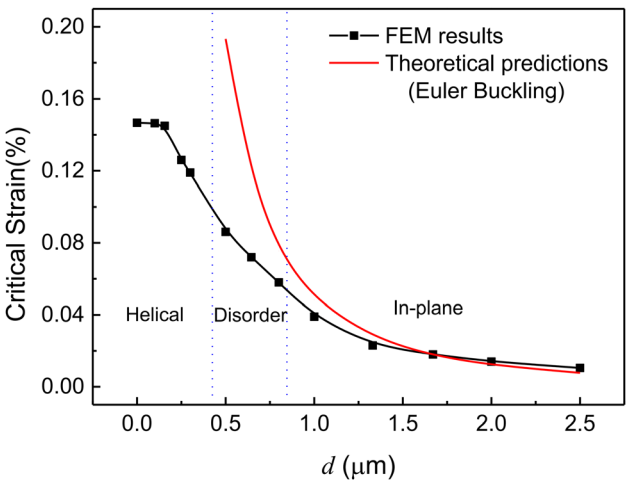

Fig. 5 The critical buckling strain of the partially bonded SiNW with different constraint densities. The smooth line (without squares) indicates the Euler beam buckling strain.

radius R, the elastic modulus E_{NW} of the SiNW, and the effective elastic modulus $\bar{E}_S$ of the PDMS substrate [20]. Here, the effective elastic modulus of the substrate is $\bar{E}_S = E_S(1-\nu_S^2)$, where E_S and ν_S are the elastic modulus and Poisson's ratio of the substrate. Such a helical model pertains when d/h is close to zero, whereas for large d/h, the buckling of the SiNW transfers to the in-plane mode.

FEM simulations are carried out to study the buckling behaviors of the SiNW on PDMS substrate via the commercial software ABAQUS. The PDMS substrate is simplified as an approximately incompressible isotropic material with Young's modulus $E_S = 3.76$ MPa and Poisson's ratio $\nu_{NW} = 0.475$ [20], and the SiNW is simplified as a beam with circular cross section. The elastic modulus and Poisson's ratio of the SiNW are $E_{NW} = 187$ GPa, $\nu_{NW} = 0.3$ [13]. The radius of SiNW is $R = 15$ nm in consistent with parallel experiments. The PDMS substrate and the SiNW are discreted by C3D8R and B31 elements, respectively. In all the FEM simulations, the length of the SiNW is 20 μm which is much longer than the buckling wavelength of the SiNW studied in this work, and the SiNW lies in the middle of the PDMS surface and far away from the surface edges (which is also consistent with the parallel experiments). Therefore, the boundary effect is regarded small. Although finite boundary is utilized in our FEM simulation, in the middle part of SiNW the buckling configuration exhibits excellent periodicity (see Fig. 7). Mesh convergence is carried out to ensure the reliability of numerical results. Different constraint densities (different d/h) are studied to explore the mechanism of the buckling mode transition.

3 Results and Discussion

3.1 Buckling Modes. The buckling modes of the SiNW for different d are shown in Fig. 2, which can be divided into three

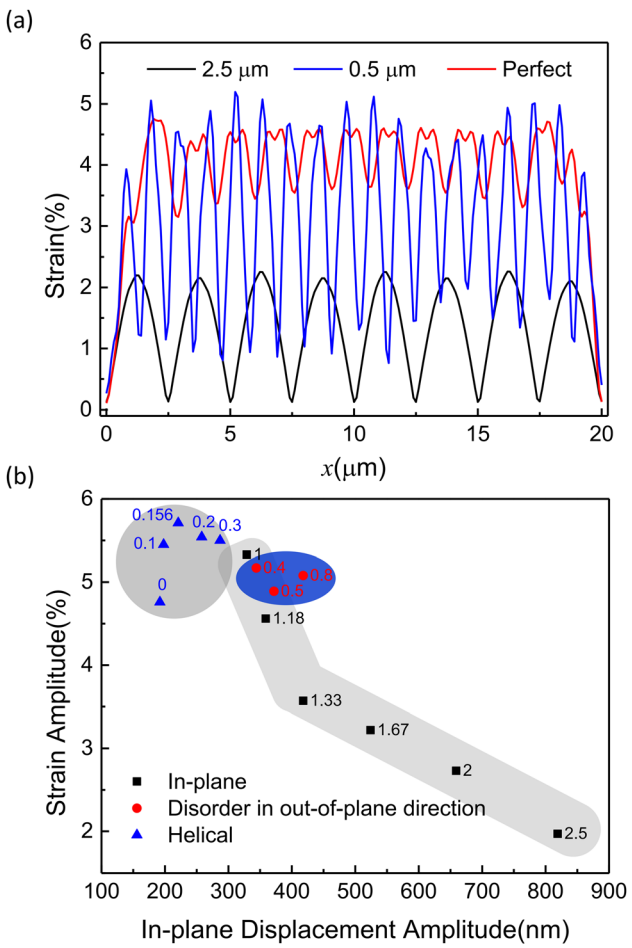

Fig. 6 (*a*) The strain distributions along SiNW for the perfectly bonded SiNW and partially bonded SiNW ($d = 2.5\ \mu$m, $d = 0.5\ \mu$m) and (*b*) the maximum strain-maximum displacement relation for different constraint densities

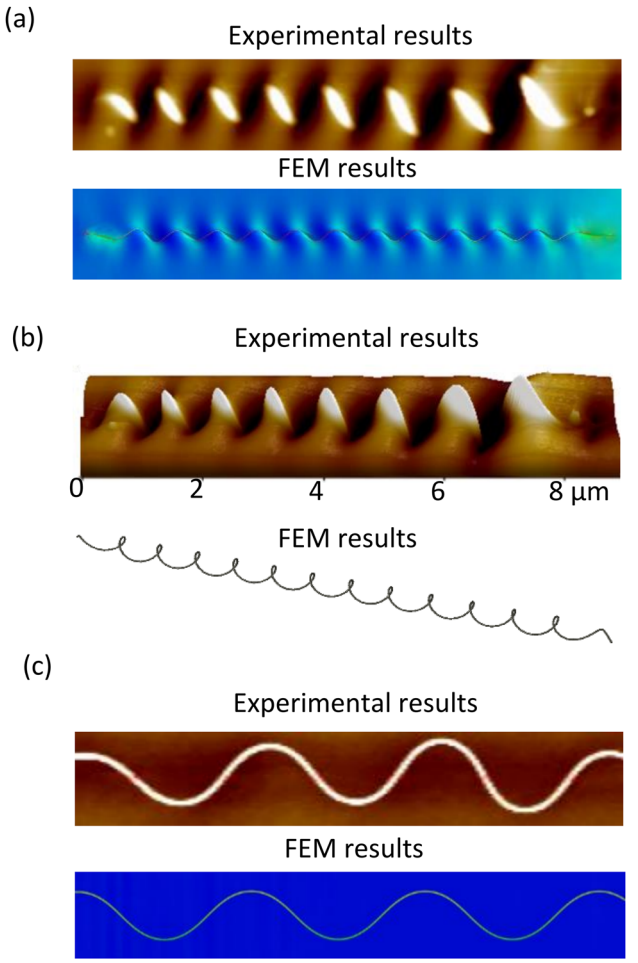

Fig. 7 The typical planar (*a*) and 3D (*b*) configuration of the SiNW for the helical buckling and (*c*) the in-plane buckling mode. The brightness represents the height of the substrate surface.

distinct regimes as the constraint density increases. When the spacing between adjacent constraint points is large enough, examples such as $d = 2.5\ \mu$m and $d = 1\ \mu$m, the buckling of the SiNW is in-plane of the PDMS substrate. The in-plane mode is sinusoidal, and the wavelength of the in-plane buckling is $2d$. The maximum strain in the SiNW locates at the maximum curvature point (middle between two constraint points), whereas the strain (as well as curvature) at the constraint point is almost zero. As the constraint density increases, e.g., $d = 0.8\ \mu$m and $d = 0.5\ \mu$m, the out-of-plane displacement of the SiNW becomes significant. The in-plane displacement is still sinusoid like, but the out-of-plane displacement is disordered. We term this mode as the disordered buckling in the out-of-plane direction. As the constraint density increases further, the configuration of the buckled SiNW becomes the helical coil, as shown for $d = 0.3\ \mu$m and $d = 0.1\ \mu$m in Fig. 2. Besides, for the helical buckling the strain distribution in the SiNW is much more uniform than that for the in-plane and disordered modes.

The corresponding in-plane and out-of-plane displacements are shown in Fig. 3 for $d = 1\ \mu$m, $d = 0.5\ \mu$m, and $d = 0.1\ \mu$m, respectively. For $d = 1\ \mu$m, the in-plane displacement is periodic and much larger than the out-of-plane displacement. While for $d = 0.5\ \mu$m, the amplitude of the out-of-plane displacement is of the same order as the in-plane displacement, however it is fairly irregular (while the in-plane component remains approximately periodic which determines the buckling wavelength). For the helical buckling ($d = 0.1\ \mu$m), the in-plane and out-of-plane displacements are similar. Nevertheless, the phase angle difference of the in-plane and out-of-plane displacements is about 90 deg, which generates the helical coil form.

The buckling spacing (or buckling wavelength for in-plane buckling) of the SiNW for different constraint densities are shown in Fig. 4, from which the three regimes are obvious. For the in-plane mode, the buckling wavelength is exactly $2d$. While for the disordered mode the relationship between the buckling spacing and the distance d is not monotonous. As the distance d approaches to zero, the profile of the SiNW transfers to the helical buckling, whose wavelength approaches to the theoretical prediction of a perfectly bonded SiNW, $h = 7.89R(E_{\mathrm{NW}}/\bar{E}_{\mathrm{S}})^{1/4}$. Substituting the parameters used in the present FEM simulation, the theoretical helical buckling spacing is $h = 1.64\ \mu$m. Further parametric studies show that the buckling mode of the SiNW is mainly governed by the ratio d/h. For $d/h > 0.50$, it is the in-plane buckling and for $0.27 < d/h < 0.50$, it is the disordered mode. While, for roughly $d/h < 0.27$, the buckling of the SiNW is predominantly helical.

The critical buckling strain, namely the compressive strain applied to the PDMS substrate when the SiNW buckling initiates, is shown in Fig. 5. For the in-plane mode, the buckling behavior between adjacent constraint points is analogous to that of a simple supported beam with length d. Based on the Euler buckling theory, the initial buckling strain for a circular beam with radius R is $(\pi R/2d)^2$, which reasonably fits the simulated buckling strain of the in-plane modes. As the constraint density increases, the critical buckling strain gradually diverges from the Euler beam theory, so as to keep a lower strain energy upon buckling. With further increasing the constraint density, the behavior approaches to that

of a perfectly bonded SiNW and the initial buckling strain is independent on the distance d.

3.2 Strain Distribution in SiNW. The strain distribution in the SiNW is another important factor that influences the performance of the stretchable electronics. For example, fracture may initiate at the largest strain point and the electrical properties of the SiNW are also affected by the strain in it [23,24]. The strain distribution along the axis of the SiNW is shown in Fig. 6(*a*) for different constraint densities $d = 2.5\ \mu$m, $d = 0.5\ \mu$m, and $d = 0\ \mu$m. Here, the strain represents the maximum principal in the cross section of the SiNW. The strain distribution for the in-plane mode ($d = 2.5\ \mu$m, for example) fluctuates with the maximum value attained at the middle of two adjacent constraint points, and the minimum value at the constraints. For the disordered mode (e.g., $d = 0.5\ \mu$m), the strain fluctuation is more severe with the maximum exceeding 5% and minimum below 2%. Relatively speaking, the strain distribution in the helical mode is more uniform and oscillates, whose maximum 4.76% is slightly smaller than the disordered mode.

A map of the amplitudes of the maximum strain and the maximum in-plane displacement is given in Fig. 6(*b*); in each case d is denoted. Generally, the strain amplitude increases as the constraint density increases. In contrast, the displacement amplitude decreases. For the in-plane buckling mode, it has smaller strain, but has larger displacement, so that larger space is required and the density of the SiNW is limited. While for the helical buckling mode it has the smallest displacement and moderate strain amplitude, which might be beneficial for stretchable electronics.

3.3 Comparison to Experiments. Parallel experiment is carried out with details outlined in previous literature [4]. For the SiNW-PDMS system without UVO treatment or less UVO treatment time (<3 min), the buckling mode of the SiNW is the in-plane which fits the prediction from FEM for a partially bonded SiNW ($d = 1\ \mu$m), as shown in Fig. 7(*c*). When the UVO treatment time is between 5 and 8 min (when strong adhesion is likely to present), the buckling of the SiNW is the helical mode which is also consistent with the FEM simulation for a perfectly bonded SiNW, as shown in Figs. 7(*a*) and 7(*b*). However, when the UVO treatment time is longer than 8 min, the mode changes to in-plane again, because the UVO treatment weakens the compliance of the PDMS near the surface which may debond.

For the in-plane mode, the surface of the PDMS substrate remains very smooth, which indicates the sliding between the SiNW and the PDMS substrates. The relationships of the in-plane displacement and out-of-plane displacement amplitudes to the effective compressive strain are given in Fig. 8. Both displacement amplitudes observed in the experiments are within the ranges of the FEM results for the helical buckling ($d = 0.25\ \mu$m, $d = 0.1\ \mu$m and perfectly bonded SiNW, $d = 0\ \mu$m), as shown in Fig. 8(*b*). This indicates that the partial debonding of the SiNW is the major reason for the transition from the in-plane buckling to the helical buckling. Due to the absence of van der Waals force in our model, the present study cannot yet precisely reproduce every feature in the experiment, nevertheless the mechanism of transition of distinctive buckling modes is elucidated.

In order to explore the underlying mechanism of the buckling mode transition for different constraint densities, the strain energy of the three different buckling modes (in-plane, disorder and helical) for three different constraint distances, 2.5 μm, 0.5 μm, and 0.1 μm, is shown in Fig. 9. Here, in order to obtain the in-plane buckling mode for the constraint distance 0.5 μm and 0.1 μm, the out-of-plane displacement of the SiNW is constrained. As shown in Fig. 9, for the constraint distance 0.5 μm, the strain energy of the in-plane buckling mode is larger than that of the out-of-plane buckling mode. Besides, the strain energy of the out-of-plane disordered buckling mode for the constraint distance 0.5 μm is

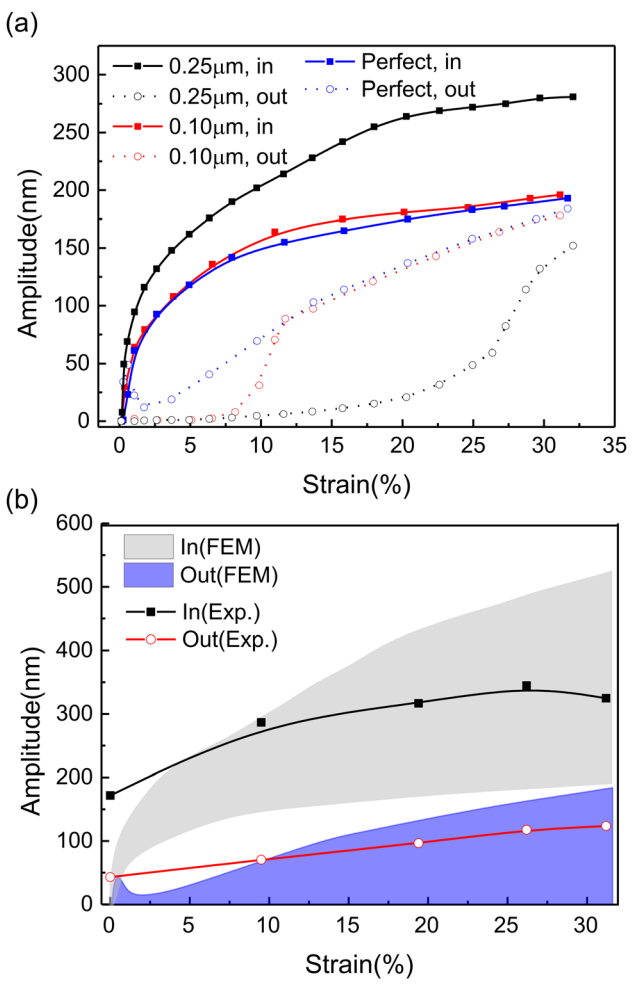

Fig. 8 (*a*) The relations of the in-plane and out-of-plane displacement amplitudes to the effective compressive strain for the helical buckling obtained from FEM simulations. (*b*) The comparison of the in-plane and the out-of-plane displacement amplitudes between experiments (up various UVO treatment time) and FEM simulations. The shadow areas indicate the ranges obtained from FEM simulations.

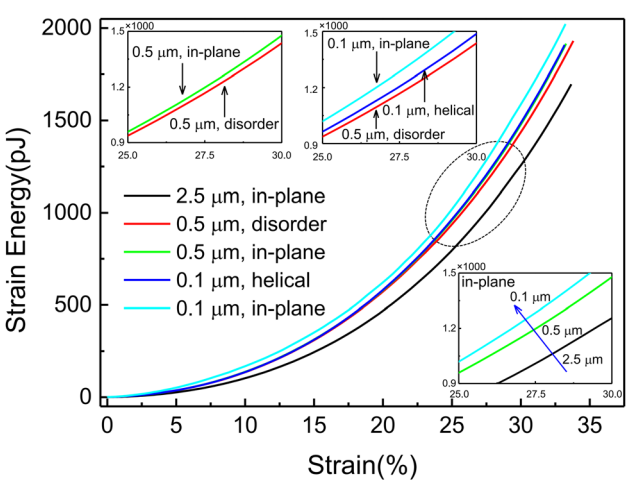

Fig. 9 The strain energy of three buckling modes for the constraint distance 2.5 μm, 0.5 μm and 0.1 μm, respectively. For the constraint distance 0.5 μm, the strain energy of the in-plane bucking mode is almost overwritten by the strain energy of the helical buckling mode with the constraint distance 0.1 μm.

smaller than that of the helical buckling mode for the constrain distance 0.1 μm. However, for the constraint distance 0.1 μm, the strain energy of the helical buckling mode is smaller than that of the in-plane buckling mode. Note that we cannot generate the helical buckling mode for the constraint distance 0.5 μm and the out-of-plane disordered bucking mode for the constraint distance 0.1 μm. Here, we cannot directly compare the strain energy between the out-of-plane disordered mode and the helical buckling mode for the constraint distance 0.5 μm and 0.1 μm. Nevertheless, it infers that the out-of-plane disordered buckling mode is energetically more favorable than the in-plane buckling mode for $0.27 < d/h < 0.5$ and the helical buckling mode is energetically more favorable for $d/h < 0.27$. In our future work, the underlying mechanism of the buckling mode transition for a nanowire on the elastomeric substrate will be systematically studied.

It should to be noted that our FEM model is a simplification to the buckling process. In the experiments, the debonding of the SiNW is accompanied by the buckling of the SiNW, while in our FEM simulation we assume the debonding occurs prior to the buckling. Moreover, the constraints in experiments may be small segments instead of singular points. In the future work we will systematically study the debonding characteristics of the SiNW and its influence to the buckling behaviors of the SiNW. Besides, the mechanical properties of the PDMS, especially near the surface of the substrate, are influenced by the UVO treatment, for example, increasing the stiffness and decreasing the deformability of the PDMS. In the future work, the gradient of the mechanical properties near the surface of the PDMS will be factored into approach.

4 Conclusion

In this work, we study the transition from the in-plane buckling to the helical buckling for the SiNW on the PDMS substrate via FEM simulations and experiments. The partial detachment of SiNW from the PDMS substrate is mainly responsible for the transition of the buckling modes, which is dictated by the ratio d/h. For $d/h > 0.50$, the buckling of the SiNW is the in-plane which can be described by the Euler beam buckling theory with the buckling wavelength $\lambda = 2d$. For $0.27 < d/h < 0.50$, the buckles are disordered in the out-of-plane direction and the critical buckling strain gradually diverges from the Euler beam theory. Whereas, for $d/h < 0.27$, the buckling is helical and the buckling spacing gradually approaches to the theoretical value of a perfectly bonded SiNW. Generally, for the in-plane buckling the strain amplitude in the SiNW gradually increases and the displacement amplitude gradually decreases with increasing the constraint density. The helical buckling of the perfectly bonded SiNW induces moderate strain, but consumes the smallest space. Therefore, an optimal design can be balanced between the strain in the SiNW and its accommodating space.

Acknowledgment

The authors acknowledge the support from the National Natural Science Foundation of China (11302163, 11372241 and 11572238), Advanced Research Projects Agency-Energy ARPA-E (DE-AR0000396) and Air Force Office of Scientific Research AFOSR (FA9550-12-1-0159). Y.Z. gratefully acknowledges the support from the National Science Foundation through Award No. CMMI-1301193. The authors thank Dr. Feng Xu for the AFM images of the coiled SiNWs.

Nomenclature

d = the distance between adjacent constraint points
$\bar{E}_S$ = effective elastic modulus of PDMS substrates
E_S = elastic modulus of substrates
E_{NW} = elastic modulus of nanowires
h = theoretical buckling spacing
R = the radius of nanowires
ν_{NW} = Poisson's ratio of nanowires
ν_S = Poisson's ratio of substrates

References

[1] Zhang, Y., Yan, Z., Nan, K., Xiao, D., Liu, Y., Luan, H., Fu, H., Wang, X., Yang, Q., Wang, J., Ren, W., Si, H., Liu, F., Yang, L., Li, H., Wang, J., Guo, X., Luo, H., Wang, L., Huang, Y., and Rogers, J. A., 2015, "A Mechanically Driven Form of Kirigami as a Route to 3D Mesostructures in Micro/Nanomembranes," Proc. Natl. Acad. Sci. U.S.A., **112**(38), pp. 11757–11764.

[2] Xu, S., Yan, Z., Jang, K. I., Huang, W., Fu, H. R., Kim, J., Wei, Z., Flavin, M., McCracken, J., Wang, R., Badea, A., Liu, Y., Xiao, D. Q., Zhou, G. Y., Lee, J., Chung, H. U., Cheng, H. Y., Ren, W., Banks, A., Li, X. L., Paik, U., Nuzzo, R. G., Huang, Y. G., Zhang, Y. H., and Rogers, J. A., 2015, "Assembly of Micro/Nanomaterials Into Complex, Three-Dimensional Architectures by Compressive Buckling," Science, **347**(6218), pp. 154–159.

[3] Yao, S., and Zhu, Y., 2015, "Nanomaterial-Enabled Stretchable Conductors: Strategies, Materials and Devices," Adv. Mater., **27**(9), pp. 1480–1511.

[4] Xu, F., Lu, W., and Zhu, Y., 2011, "Controlled 3D Buckling of Silicon Nanowires for Stretchable Electronics," ACS Nano, **5**(1), pp. 672–678.

[5] Kim, D.-H., and Rogers, J. A., 2009, "Bend, Buckle, and Fold: Mechanical Engineering With Nanomembranes," ACS Nano, **3**(3), pp. 498–501.

[6] Song, J., Jiang, H., Huang, Y., and Rogers, J. A., 2009, "Mechanics of Stretchable Inorganic Electronic Materials," J. Vac. Sci. Technol., A, **27**(5), p. 1107.

[7] Rogers, J. A., Someya, T., and Huang, Y., 2010, "Materials and Mechanics for Stretchable Electronics," Science, **327**(5973), pp. 1603–1607.

[8] Song, J., Huang, Y., Xiao, J., Wang, S., Hwang, K. C., Ko, H. C., Kim, D. H., Stoykovich, M. P., and Rogers, J. A., 2009, "Mechanics of Noncoplanar Mesh Design for Stretchable Electronic Circuits," J. Appl. Phys., **105**(12), p. 123516.

[9] Chen, X., and Yin, J., 2010, "Buckling Patterns of Thin Films on Curved Compliant Substrates With Applications to Morphogenesis and Three-Dimensional Micro-Fabrication," Soft Matter, **6**(22), pp. 5667–5680.

[10] Zhong, Z., Wang, D., Cui, Y., Bockrath, M. W., and Lieber, C. M., 2003, "Nanowire Crossbar Arrays as Address Decoders for Integrated Nanosystems," Science, **302**(5649), pp. 1377–1379.

[11] Holmes, J. D., Johnston, K. P., Doty, R. C., and Korgel, B. A., 2000, "Orientation of Solution-Grown Silicon Nanowires," Science, **287**(5457), p. 1471.

[12] Wu, Y., Xiang, J., Yang, C., Lu, W., and Lieber, C. M., 2004, "Single-Crystal Metallic Nanowires and Metal/Semiconductor Nanowire Heterostructures," Nature, **430**(6995), pp. 61–65.

[13] Zhu, Y., Xu, F., Qin, Q., Fung, W. Y., and Lu, W., 2009, "Mechanical Properties of Vapor-Liquid-Solid Synthesized Silicon Nanowires," Nano Lett., **9**(11), pp. 3934–3939.

[14] Hoffmann, S., Utke, I., Moser, B., Michler, J., Christiansen, S. H., Schmidt, V., Senz, S., Werner, P., Gösele, U., and Ballif, C., 2006, "Measurement of the Bending Strength of Vapor-Liquid-Solid Grown Silicon Nanowires," Nano Lett., **6**(4), pp. 622–625.

[15] Ryu, S. Y., Xiao, J., Park, W. I., Son, K. S., Huang, Y. Y., Paik, U., and Rogers, J. A., 2009, "Lateral Buckling Mechanics in Silicon Nanowires on Elastomeric Substrates," Nano Lett., **9**(9), pp. 3214–3219.

[16] Xiao, J., Ryu, S. Y., Huang, Y., Hwang, K. C., Paik, U., and Rogers, J. A., 2010, "Mechanics of Nanowire/Nanotube In-Surface Buckling on Elastomeric Substrates," Nanotechnology, **21**(8), p. 85708.

[17] Durham, J. W., 3rd, and Zhu, Y., 2013, "Fabrication of Functional Nanowire Devices on Unconventional Substrates Using Strain-Release Assembly," ACS Appl. Mater. Interfaces, **5**(2), pp. 256–261.

[18] Qin, Q., and Zhu, Y., 2011, "Static Friction Between Silicon Nanowires and Elastomeric Substrates," ACS Nano, **5**(9), pp. 7404–7410.

[19] Efimenko, K., Wallace, W. E., and Genzer, J., 2002, "Surface Modification of Sylgard-184 Poly(Dimethyl Siloxane) Networks by Ultraviolet and Ultraviolet/Ozone Treatment," J. Colloid Interface Sci., **254**(2), pp. 306–315.

[20] Chen, Y., Liu, Y., Yan, Y., Zhu, Y., and Chen, X., "Helical Coil Buckling Mechanism for a Stiff Nanowire on an Elastomeric Substrate," (unpublished work).

[21] Xiao, J., Jiang, H., Khang, D. Y., Wu, J., Huang, Y., and Rogers, J. A., 2008, "Mechanics of Buckled Carbon Nanotubes on Elastomeric Substrates," J. Appl. Phys., **104**(3), p. 033543.

[22] Duan, Y., Huang, Y., and Yin, Z., 2015, "Competing Buckling of Micro/Nanowires on Compliant Substrates," J. Phys. D: Appl. Phys., **48**(4), p. 045302.

[23] Peng, X. H., Alizadeh, A., Kumar, S. K., and Nayak, S. K., 2009, "Ab Initio Study of Size and Strain Effects on the Electronic Properties of Si Nanowires," ASME Int. J. Appl. Mech., **1**(3), pp. 483–499.

[24] Sajjad, R. N., and Alam, K., 2009, "Electronic Properties of a Strained <100> Silicon Nanowire," J. Appl. Phys., **105**(4), p. 044307.